Available online at www.sciencedirect.com
ScienceDirect
International Journal of Pharmaceutics 333 (2007) 177–186
INTERNATIONAL JOURNAL OF PHARMACEUTICS
www.elsevier.com/locate/ijpharm

Pharmaceutical Nanotechnology

# Preparation and characterization of superparamagnetic iron oxide nanoparticles stabilized by alginate

Hui-li Ma [a], Xian-rong Qi [a,*], Yoshie Maitani [b], Tsuneji Nagai [b]

[a] *Department of Pharmaceutics, School of Pharmaceutical Sciences, Peking University, Beijing 100083, China*
[b] *Institute of Medicinal Chemistry, Hoshi University, Shinagawa-Ku, Tokyo 142-850, Japan*

Received 8 June 2006; received in revised form 27 September 2006; accepted 2 October 2006
Available online 7 October 2006

**Abstract**

SPION with appropriate surface chemistry have been widely used experimentally for numerous in vivo applications. In this study, SPION stabilized by alginate (SPION-alginate) were prepared by a modified coprecipitation method. The structure, size, morphology, magnetic property and relaxivity of the SPION-alginate were characterized systematically by means of XRD, TEM, ESEM, AFM, DLS, SQUID magnetometer and MRI, respectively, and the interaction between alginate and iron oxide ($Fe_3O_4$) was characterized by FT-IR and AFM. The results revealed that typical iron oxide nanoparticles were $Fe_3O_4$ with a core diameter of 5–10 nm and SPION-alginate had a hydrodynamic diameter of 193.8–483.2 nm. From the magnetization curve, the Ms of a suspension of SPION-alginate was 40 emu/g, corresponding to 73% of that of solid SPION-alginate. This high Ms may be due to the binding of $Fe_3O_4$ nanoparticles to alginate macromolecule strands as visually confirmed by AFM. SPION-alginate of several hundred nanometers was stable in size for 12 months at 4 °C. Moreover, T1 relaxivity and T2 relaxivity of SPION-alginate in saline (1.5 T, 20 °C) were $7.86 \pm 0.20\ s^{-1}\ mM^{-1}$ and $281.2 \pm 26.4\ s^{-1}\ mM^{-1}$, respectively.


*Keywords:* Alginate; Superparamagnetic iron oxide nanoparticles (SPION); Magnetometric; Atomic force microscopy (AFM); Magnetic resonance imaging (MRI)

## 1. Introduction

Alginate, a natural-occurring polyelectrolytic polysaccharide found in all species of brown algae and some species of bacteria, is a linear polymer composed of α-L-guluronate (G) and β-D-mannuronate (M) units in varying proportions and sequential arrangements, and is biocompatible and biodegradable in tissue (Gombotz and Wee, 1998; Robitaille et al., 1999; Bouhadir et al., 2001). Alginates have also been widely studied for their ability to form gels in the presence of divalent cations (Nesterova et al., 2000; Finotelli et al., 2004; Sreeram et al., 2004). Metal alginate gels are ionotropic in nature, differing from the classical type of gels in which long-chain molecules are held together by simple van der Waals forces, and the macromolecular chains are chelating polyvalent metal ions (Khairou et al., 2002). The design and construction of metal-containing nanoscale arrays is a challenge since such structures are expected to be indispensable in the emerging technologies of this century.

Superparamagnetic iron oxide nanoparticles (SPION) with appropriate surface chemistry have been widely used experimentally applications such as magnetic resonance imaging contrast enhancement (Wang et al., 2001), immunoassay (Medina et al., 2004), hyperthermia (Jordan et al., 2001), magnetic drug delivery (Alexiou et al., 2000), magnetofection (Krotz et al., 2003), cell separation/cell labelling (Olsvik et al., 1994; Bulte et al., 2001), etc. Furthermore, some SPION preparations have already been approved for clinical use, especially for MR imaging, such as Endorem® (diameter 80–150 nm, Advanced Magnetics) and Resovist® (diameter 60 nm, Schering) for liver/spleen imaging (Wang et al., 2001). Recently, functionalized magnetic nanoparticles conjugated with antibodies or receptors including epidermal growth factor receptors (EGFRs) (Suwa et al., 1998), her2/neu (Funovics et al., 2004) and folate (Sonvico et al., 2005)

*Abbreviations:* SPION, superparamagnetic iron oxide nanoparticles; XRD, X-ray diffraction; TEM, transmission electron microscopy; ESEM, environmental scanning electron microscopy; AFM, atomic force microscopy; DLS, dynamic light scattering; SQUID, superconducting quantum interference device; MRI, magnetic resonance image; FT-IR, Fourier transform infrared spectroscopy; Ms, saturation magnetizations

* Corresponding author. Tel.: +86 10 82801584; fax: +86 10 82802791.
*E-mail address:* qixr2001@yahoo.com.cn (X.-r. Qi).

0378-5173/$ – see front matter © 2006 Elsevier B.V. All rights reserved.
doi:10.1016/j.ijpharm.2006.10.006

have been widely studied. These applications need special surface coating of the magnetic particles, which has to be not only non-toxic and biocompatible but also allow targetable delivery with particle localization in a specific area. Most work in this field has been done to improve the biocompatibility of the materials, but only a few scientific investigations and developments have been carried out to improve the quality of magnetic particles, their size distribution, their shape and surface so as to characterize them to establish a protocol for their quality control. The nature of surface coatings and their subsequent geometric arrangement on nanoparticles determine not only the overall size of the colloid but also play a significant role in the biokinetics and biodistribution of nanoparticles in the body. Some authors have reviewed the different factors related to the clearance of the iron oxide nanoparticles from blood: particle size, dose, surface charge, coating material, stability in physiological environment, etc. (Gupta and Gupta, 2005). According to the previous studies, the particle size plays a very important effect. The larger the particles, the shorter their plasma half-life. The blood half-life of AMI-25 with a diameter of 80–150 nm is only 6 min and approximately 80% of the injected dose accumulated in the liver and 5–10% in the spleen within minutes of administration. However, the vascular half-life of NC10050 with diameter of 20 nm was up to 3–4 h (Wang et al., 2001). It was reported that the higher the surface charge, the shorter the residence time of SPION in the circulation (Neuberger et al., 2005).

In recent years, several investigations for the preparation of iron oxide nanoparticles with alginate have been developed (Kroll et al., 1996; Llanes et al., 2000; Shen et al., 2003; Nishio et al., 2004). The standard chemical synthesis consists of three steps: (a) gelation of alginate and ferrous ion; (b) in situ precipitation of ferrous hydroxide by the alkaline treatment of alginate; (c) oxidation of ferrous hydroxide with an oxidizing agent such as $O_2$ or $H_2O_2$. The methods mentioned above are complex, since it involves multiple recycles to produce iron oxide of about 50% content, needs control of the complicated oxidation reaction, and usually results in a nonmagnetic form of iron oxide. Moreover, the way alginate interacts with iron ions has not yet well been understood. It has been considered that the alginate polymeric backbone is more conformationally restricted and hence it would result in the aggregation of iron (Sreeram et al., 2004). Thus, we attempt to develop a modified two-step coprecipitation method, involving (a) formation of $Fe_3O_4$ particles by coprecipitation of ferric and ferrous ion with alkaline solution, and (b) combination of $Fe_3O_4$ particles to alginate. Compared with the standard chemical synthesis method, the preparation process is easier and SPION-alginate produced by this method will be of good stability and good magnetism. It was reported that the reason for the stability of dextran-coated iron oxide particles was that a $COO^-$ terminal of dextran bound to a Fe atom on the core surface (Kawaguchi et al., 2001). Electrostatic repulsion between particles with the same electric charge prevents the aggregation of particles (Ravi Kumar et al., 2004). Meanwhile, alginate has the structure with many carboxyl groups as mentioned above. Hence, we speculated the interaction between $COO^-$ of alginate and iron ion as well as the electrostatic repulsion may make the SPION-alginate stable.

This study reports our efforts to understand the nature of the iron ion-alginate of SPION-alginate and to develop a SPION-alginate composite, which may be an application in magnetic resonance imaging.

## 2. Experimental

### 2.1. Materials

Three kinds of sodium alginate of pharmaceutical grade, KELTONE® LVCR (with a viscosity average molecular weight of 54,000 and an M/G ratio of 1.5), KELTONE® HVCR (with a viscosity average molecular weight of 160,000 and an M/G ratio of 1.5) and MANUGEL® DMB (with a viscosity average molecular weight of 124,000 and an M/G ratio of 0.6), were kindly donated by ISP Alginate Inc. Ferric chloride hexahydrate, ferrous chloride tetrahydrate and all other chemicals used for this study were of analytical grade with no further purification.

### 2.2. Preparation of $Fe_3O_4$ particles and SPION-alginate

SPION-alginate was prepared by coprecipitation of ferric and ferrous ion with sodium hydroxide (NaOH). The ferric and ferrous chlorides (molar ratio of 2:1.5) were dissolved in distilled water and chemical precipitation was achieved by adding 5 mol $l^{-1}$ NaOH solution at 60 °C. Fifty microliters of sodium alginate solution was added to the suspension and was stirred vigorously for 30 min. The mixture was heated at 80 °C with slow stirring for 1 h and then sonicated for 20 min. All the above processes were run under total $N_2$ protection. The obtained suspension was dialyzed against deionized water with water replacement until there was no $FeCl_2$ or $FeCl_3$ in the dialysate identified by 0.1 mol $l^{-1}$ of $AgNO_3$ solution. Then the suspension was centrifuged at 10,000 rpm for 20 min to remove the solid material and the black supernatant, namely SPION-alginate, was collected. A fraction of SPION-alginate was dried with a rotary evaporator at 50 °C to obtain a membranous solid sample and then the solid sample was used for XRD, SQUID and FT-IR analyses.

$Fe_3O_4$ particles without alginate were also prepared as described above, except that the solution was distilled water instead of sodium alginate solution.

### 2.3. Content determination of $Fe_3O_4$ in SPION-alginate

The content of $Fe_3O_4$ in the suspension and solid sample of SPION-alginate was determined by *o*-phenanthroline method after 37.5% HCl acidation (Hagar et al., 2003).

### 2.4. Particle structure analysis of SPION-alginate

XRD (APD-10, Philips, Netherlands) was performed to identify the structure of the SPION-alginate using Cu Kα radiation ($\lambda = 1.54056$ Å) between 20° and 90° ($2\theta$) at 27 °C.

### 2.5. Particle size, morphology and ξ-potential analysis

The size and morphology of $Fe_3O_4$ nanoparticles in the SPION-alginate were observed by TEM (JEM-1230, JEOL, Japan) and ESEM (QUANTA 200F, FEI, USA). The sample for TEM analysis was obtained by placing a drop of SPION-alginate suspension diluted by distilled water onto a copper grid without any staining, and drying it in air at room temperature. For ESEM analysis, the SPION-alginate was freeze-dried for 24 h to obtain solid samples.

The average hydrodynamic radius and the ξ-potential of alginate solution and SPION-alginate were determined by DLS (Zetasizer ZEN 3600, Malvern, UK). All DLS measurements were done with an angle detection of 90° at 25 °C after diluting the dispersion to an appropriate volume with water. The results were the mean values of two experiments using the same sample.

### 2.6. AFM analysis

The size and surface topography of alginate macromolecules (LVCR) and alginate-$Fe_3O_4$ nanoparticles in SPION-alginate were analyzed by AFM with E-Scanner (NanoScope IV, Veeco, USA). Measurements were performed both in liquid and in air. The concentration of alginate in the alginate solution and SPION-alginate was 0.0625% (w/w). For AFM analysis in liquid, 10 μl of the alginate solution or SPION-alginate was deposited onto freshly cleaved sheets of mica surface, and then an image was made in contact mode with a V-shaped silicon nitride probe and a spring constant of 0.32 N/m. For AFM analysis in air, 10 μl of the alginate solution or the SPION-alginate was deposited briefly onto the newly cleaved mica surface, the surface was air-dried in a dust-free enclosure for 24 h and was imaged in Tapping model Etched Silicon Probe (TESP) with a spring constant of about 20–100 N/m and a resonance frequency of about 200–400 kHz. All the images were examined by Nanoscope Image Analysis software and underwent by section analysis and measurements, in which the "height" data type mode was used.

### 2.7. Magnetic property

Magnetic measurement was done using a SQUID magnetometer (MPMSXL-7, Quantum Design, USA). Magnetization curves were recorded for a suspension and solid sample of SPION-alginate at 27 °C with an applied magnetic field up to 10,000 Oe.

### 2.8. FT-IR analysis

The binding of $Fe_3O_4$ to alginate in a solid sample of SPION-alginate was checked by FT-IR (AVATAR 360, Nicolet, USA). FT-IR spectra were obtained with KBr pellets and the spectrum was taken from 4000–500 $cm^{-1}$.

### 2.9. MRI measurement

The T1 and T2 relaxation times (s) of the medium were measured for different concentrations of SPION-alginate at 20 °C using a 1.5 T clinical MRI scanner (GE HD, Milwaukee, WI, USA) with a quadrature transmit–receive head coil. SPION-alginate was diluted with saline before analysis to eight Fe concentrations between 0.074 mM and 0.300 mM, and the saline was taken as a control sample. $T_1$-weighted images were obtained with a multi-repetition SE sequence (TR 200 ms, 300 ms, 500 ms, 800 ms, 1200 ms; TE 9 ms; bandwidth 62.5 Hz; matrix 256 × 128; NEX 1) and $T_2$-weighted images were obtained with an FSE sequence (TR 3000 ms; TE 6.3 ms, 12.55 ms, 18.8 ms, 25.05 ms, 31.03 ms, 37.55 ms, 43.8 ms, 50.05 ms; echo train length 8; echo spacing 6.25 ms; bandwidth 62.5 Hz; matrix 256 × 128; NEX 1). In both cases, a circular region of interest was selected in each sample and the values of T1 and T2 relaxation times were obtained. The increase in R1 and R2 relaxation rates ($s^{-1}$, $1/T$) with increasing Fe concentration was analyzed by linear least squares regression analysis and correlation coefficients greater than 0.98 were obtained. T1 relaxivity and T2 relaxivity ($s^{-1}$ $mM^{-1}$) were calculated from the slope of the linear plots of R1 and R2 versus Fe concentration (Simon et al., 2006).

## 3. Results and discussion

### 3.1. Content of $Fe_3O_4$ in SPION-alginate

The $Fe_3O_4$ contents in solid samples of SPION-alginate varied with the type of alginate (Fig. 1a), but rarely changed when the concentration of alginate (LVCR) increased from 1% to 4% (w/w) (Fig. 1b). The content of $Fe_3O_4$ in SPION-alginate produced with LVCR alginate is twice as high as that produced with HVCR alginate or DMB alginate. Thus, the low molecular weight of alginate is beneficial for the formation of SPION-alginate with high iron content. The interaction between alginate and iron ions could be explained by a site-binding model, i.e. iron ions are bound to binding sites in the alginate and form spatially separated iron ion centers on the alginate backbone (Sreeram et al., 2004). So, the higher the molecular weight of alginate, the more it is conformationally restricted to form SPION-alginate with higher iron content. Furthermore, although G sequences of alginate are superior to complexes with iron ions compared to M sequences (Llanes et al., 2000), complex formation is possible with both G and M sequences since the iron content is similarly produced with LVCR alginate (M/G ratio of 1.5), HVCR alginate (M/G ratio of 1.5), or DMB alginate (M/G ratio of 0.6). In addition, the $Fe_3O_4$ content in SPION-alginate produced with 1 wt% LVCR alginate can reach to 50% (w/w). In a suspension sample of SPION-alginate, the $Fe_3O_4$ concentrations were 1–4 mg $ml^{-1}$ when prepared with LVCR alginate at concentrations of 1%, 2%, or 4% (w/w).

In this study, two steps are involved in the preparation of SPION-alginate: (1) formation of $Fe_3O_4$ by coprecipitation of ferric and ferrous ion with alkaline solution; (2) binding of alginate polymer to iron oxide. It is easier to produce $Fe_3O_4$ with higher iron oxide content and better magnetism in comparison with the methods described in Section 1, which included three steps. It is known that $Fe_3O_4$ magnetism is usually higher that that of γ-$Fe_2O_3$. Iron oxide prepared by the three-step method is

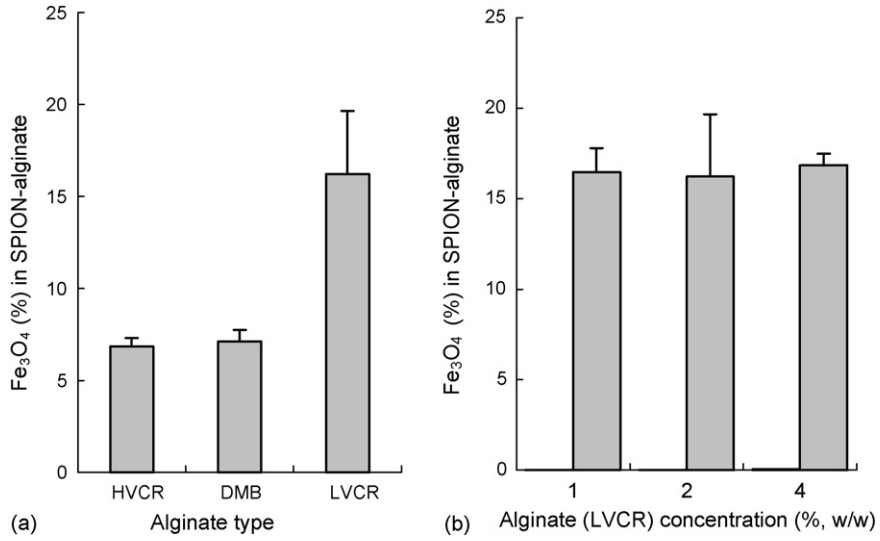


Fig. 1. The effects of alginate types (a) and alginate (LVCR) concentrations (b) on $Fe_3O_4$ content in a solid sample of SPION-alginate (mean ± S.D., three batches).

usually γ-$Fe_2O_3$ with an Ms of 30 emu/g at room temperature, and it usually results in the nonmagnetic form of iron oxide such as ferric oxyhydroxide (FeOOH) during the oxidation reaction process. Furthermore, multiple recycles are necessary to obtain iron oxide with a higher content (Kroll et al., 1996; Llanes et al., 2000; Shen et al., 2003; Nishio et al., 2004).

### 3.2. Particle structure analysis of SPION-alginate by XRD

Fig. 2 shows the XRD pattern for alginate-$Fe_3O_4$ nanoparticles. There are seven characteristic peaks of $2\theta$, 30.100, 35.640, 43.257, 53.502, 57.180, 62.820 and 73.984, and the corresponding intensities ($I$%) with height are 25.0, 100.0, 27.5, 11.1, 31.6, 59.0 and 8.6, respectively. These results revealed that the particles were $Fe_3O_4$ with a spinal structure. The peaks were broadened due to the small size of crystallites. The average diameter of the crystals (in angstroms), $D$, was calculated with the Scherrer formula, $D = \kappa\lambda/(\beta \cos\theta)$, where λ is the X-ray wavelength, $\kappa$ the shape factor, $\theta$ the Bragg angle (in degrees) and $\beta$ is line broadening measured at half-height and expressed in units of $2\theta$ (Wan et al., 1996). In the case of this XRD, $\kappa = 1$, $\lambda = 1.54056$ Å for Cu Kα source. The average particle size of $Fe_3O_4$ in the SPION-alginate was 2.6 nm from the seven Bragg angle mentioned above.

### 3.3. Particle size, morphology and ξ-potential analysis by TEM, ESEM and DLS

The typical TEM image of $Fe_3O_4$ nanoparticles in SPION-alginate is shown in Fig. 3. It was clear that the $Fe_3O_4$ particles were cubic shaped and monodispersed with a diameter of about 10 nm. The ESEM micrograph for the alginate-$Fe_3O_4$ nanoparticles in SPION-alginate in Fig. 4 indicated that the alginate-$Fe_3O_4$ nanoparticles seemed like the sponge, and $Fe_3O_4$ may be embedded in alginate substrate.

The hydrodynamic radius of SPION-alginate prepared at different concentrations of alginate (LVCR) is shown in Table 1. It is evident that the average hydrodynamic radius of SPION-alginate increased from 193.8 nm to 483.2 nm with an increasing

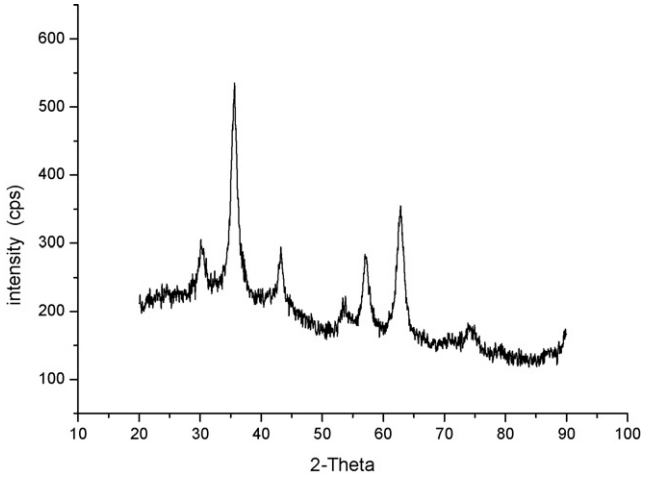


Fig. 2. X-ray diffractogram of SPION-alginate.

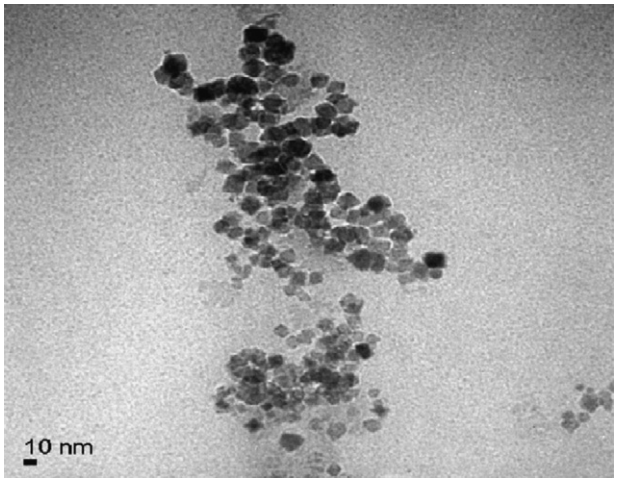


Fig. 3. TEM image of $Fe_3O_4$ nanoparticles in SPION-alginate.

Table 1
Hydrodynamic radius (*Z*-average) and ξ-potential for SPION-alginate produced with different concentrations of alginate (LVCR) after storage at 4 °C ($n = 2$)

| Time (months) | 1 | | | 5 | | 7 | | 12 | |
|---|---|---|---|---|---|---|---|---|---|
| Alginate concentration (%, w/w) | 1 | 2 | 4 | 1 | 2 | 1 | 2 | 1 | 2 |
| *Z*-average (nm) | 193.8 | 350.7 | 483.2 | 161.6 | 263.7 | 161.2 | 276.1 | 160.9 | 264.3 |
| Polydispersity | 0.209 | 0.264 | 0.204 | 0.213 | 0.217 | 0.215 | 0.216 | 0.207 | 0.116 |
| ξ-potential (mV) | −67.5 | – | – | −61.7 | −75.7 | −59.7 | −57.0 | −59.1 | −67.9 |

The ξ-potential of alginate macromolecules was −71.8 mV measured by DLS. SPION-alginate was filled with nitrogen gas to avoid oxidation. (–) Not determined.

concentration of alginate. This value seems quite large compared with the size of $Fe_3O_4$ (10 nm by TEM in Fig. 3), but it can be explained by the polydispersity of the alginate used here, because a *Z*-average hydrodynamic radius of 200–500 nm was determined for the pure alginate solution. Since the scattered light intensity shows quadratic dependence on the volume of scatterer according to the classical Rayleigh theory, the contribution of larger molecules is more pronounced in a polydisperse sample in general (Sipos et al., 2003).

In this study, the ξ-potential of SPION-alginate made with alginate (LVCR) of 1%, 2% and 4% (w/w) were in the range of −57.0 mV to −75.7 mV (Table 1), which was not significantly different from that of alginate solution (−71.8 mV). The charge of SPION-alginate may come from the carboxyl group of alginate. No sedimentation was observed in the bottle of the SPION-alginate filled with nitrogen gas even after 12 months of storage at 4 °C at pH 7.0. One of the reasons for the high stability of SPION-alginate may be the binding of the carboxyl group of alginate to iron oxide nuclei, which similar with the report of Massart et al. (Massart et al., 1995; Bee et al., 1995). It was reported that the specific adsorption of citrate anions on the ferric oxide surface can inhibit the growth of the maghemite particles and make the particles very stable over a wide range of pH. Furthermore, the ξ-potential is an important characteristic as it can influence particle stability. In theory, more pronounced ξ-potential values, no matter positive or negative, tend to stabilize particle suspension. Electrostatic repulsion between particles with the same electric charge prevents the aggregation of particles (Ravi Kumar et al., 2004). The results suggest that SPION-alginate would be stable for at least 1 year.

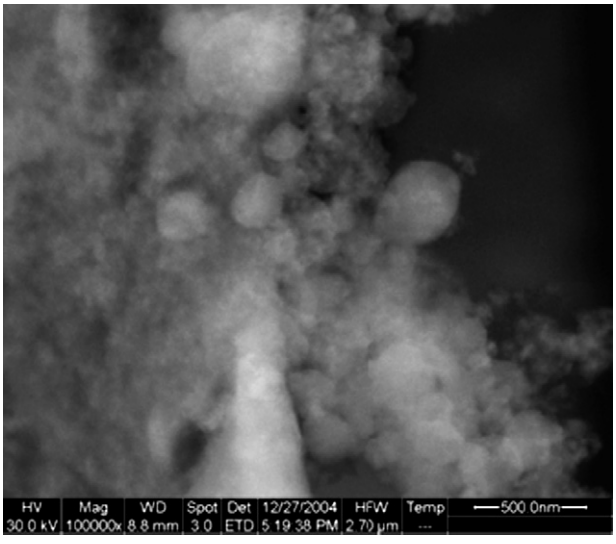


Fig. 4. ESEM micrograph of alginate-$Fe_3O_4$ nanoparticles in freeze-dried SPION-alginate.

### 3.4. AFM analysis

AFM was applied to investigate SPION-alginate in an aqueous environment. In recent years, compared to ESEM and TEM methods, AFM has appeared to be an appropriate technique for two reasons (Drake et al., 1989): (1) AFM can explore the contact lens surface in aqueous environment; (2) AFM can provide microscopic information with a spatial resolution relevant to atomic scale measurements.

AFM images for alginate macromolecules and SPION-alginate are presented in Fig. 5. We did not observe alginate macromolecules in alginate solution (Fig. 5a), which may be explained by the electric repulsion of the alginate solution and mica surface. It is well known that the surface charge of mica is negative and the ξ-potential of alginate solution is −71.8 mV (based on DLS in Table 1). The "bright point" in Fig. 5a only demonstrated that the probe had contact with the surface of mica.

As shown in Fig. 5b for alginate in air, the strands of alginate macromolecules seemed like "branches" of a tree. Tracing across individual alginate strands provided an estimate of width of the alginate macromolecules, by measuring the molecular height relative to the mica surface. The results showed that the average width of a single strand is 2.729 nm (Table 2), which was consistent with the size determined by others (Decho, 1999). In Fig. 5c for SPION-alginate in liquid, the "bright spot" can be inferred to be iron oxide, the average size of which is 4.678 nm (Table 2). The observed variability in the width of alginate molecules may be explained by the physical structure of the molecules. The two monomers G and M are arranged as a series of block structures including M-blocks (-M-M-M-M), G-blocks (-G-G-G-G) and M-G-blocks (-M-G-M-G). When an M-G-block is present, there is an abrupt right angle change in the orientation of the polymer molecules. Consequently, "kinks" as in Fig. 5b may correspond to -M-G- linkages. As shown in Fig. 5d for SPION-alginate in air, it is clear that $Fe_3O_4$ nanoparticles bind to the strands of alginate macromolecules. We speculate that the $COO^-$ terminal of alginate macromolecules may bind $Fe_3O_4$ nanoparticles. Meanwhile, it was found that some alginate macromolecules formed an "egg-box" structure as a result of interactions between alginate macromolecules and iron ions of $Fe_3O_4$ particles. On the other hand, the measured average size of $Fe_3O_4$ is 7.530 nm (Table 2) in air, larger than 4.678 nm

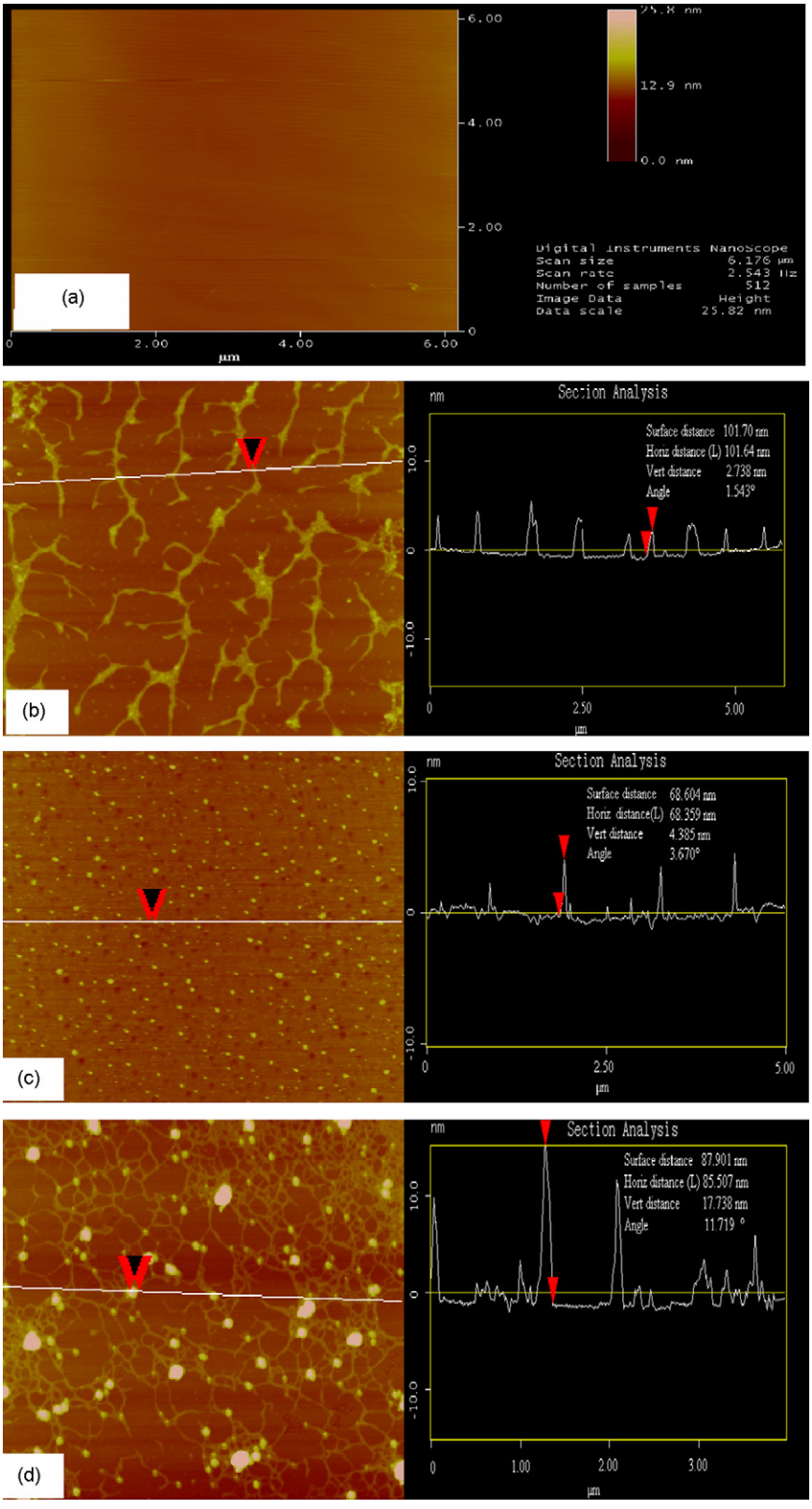


Fig. 5. Topographic images by AFM and corresponding section analysis of (a) alginate (LVCR) solution with contact model; (b) alginate (LVCR) in air with tapping model; (c) SPION-alginate in liquid with contact model; (d) SPION-alginate in air with tapping model. The thickness of alginate strands and size of $Fe_3O_4$ nanoparticles in SPION-alginate are measured by height (nm) on the *y*-axis (vertical). Arrows represent markers for width measurements (section analysis).

Table 2
The average size of alginate macromolecules in air, $Fe_3O_4$ nanoparticles in SPION-alginate in liquid and $Fe_3O_4$ nanoparticles in SPION-alginate in air determined by AFM

| Sample | Substrate depth (nm) | Threshold height (nm) | Grain height[a] (nm) |
|---|---|---|---|
| Alginate macromolecules in air | 12.781 | 1.564 | 2.729 |
| $Fe_3O_4$ nanoparticles in SPION-alginate in liquid | 9.840 | 2.567 | 4.678 |
| $Fe_3O_4$ nanoparticles in SPION-alginate in air | 51.022 | 4.154 | 7.530 |

[a] The "grain height" notes the average size of the sample in Fig. 5.

measured in liquid, indicating that some $Fe_3O_4$ nanoparticles aggregated slightly, which may be caused by the drying process.

### 3.5. Magnetic property

Magnetization curves (*M–H* loop) for the suspension and solid sample of SPION-alginate at 300 K are illustrated in Fig. 6. Magnetization did not reach saturation, even at the maximum applied magnetic field of 10,000 Oe, and no hysteresis was found, which indicated that the nanoparticles were superparamagnetic (Shafi et al., 1998; Vijayakumar et al., 2000). This could be attributed to the fact that the magnetic nanoparticles were so small that they may be considered to have a single magnetic domain. It has been reported that single domains of maghemite, γ-$Fe_2O_3$, or magnetite, $Fe_3O_4$ are about 5–20 nm in diameter (Gupta and Gupta, 2005). Therefore, the size of $Fe_3O_4$ nanoparticles in this study was inferred to be around 5–10 nm, consistent with the results of TEM observation (about 10 nm in Fig. 3), AFM analysis (4.678 nm in liquid and 7.530 nm in air in Fig. 5) and the calculated value of XRD (2.6 nm in Fig. 2) using Scherrer's formula. From the magnetization curve, the Ms of the solid samples with $Fe_3O_4$ content of 12.5% and 47.0% were 55 emu/g and 52 emu/g, respectively, while the Ms of corresponding suspension samples with $Fe_3O_4$ content of 1.09 mg $ml^{-1}$ and 3.02 mg $ml^{-1}$ were 40 emu/g and 38 emu/g, respectively. Therefore, the Ms of suspension samples were both 73% of solid samples.

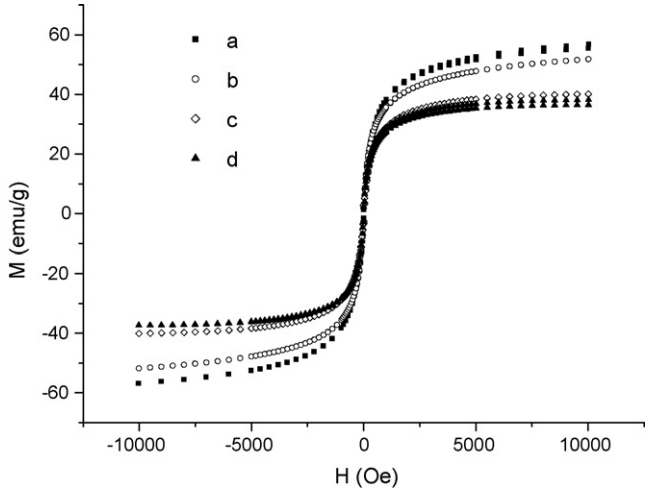


Fig. 6. Magnetization curve (*M–H*) of SPION-alginate at 27 °C. (a) Solid sample with $Fe_3O_4$ content of 12.5%; (b) solid sample with $Fe_3O_4$ content of 47.0%; (c) suspension sample with $Fe_3O_4$ content of 1.09 mg $ml^{-1}$; (d) suspension sample with $Fe_3O_4$ content of 3.02 mg $ml^{-1}$.

Compared with the Ms of bulk $Fe_3O_4$ (92 emu/g), the Ms of SPION-alginate (55 emu/g) was lower, which might be attributed to the decreased particle size and the concomitant increase in surface area. It is known that the energy of a magnetic particle in an external field is proportional to its size via the number of magnetic molecules in a single magnetic domain. When this energy becomes comparable to thermal energy, thermal fluctuations will significantly reduce the total magnetic moment in a given field (Upadhyay et al., 1995; Shafi et al., 1998; Vijayakumar et al., 2000). Therefore, the magnetic properties of nanoparticles are usually smaller than those of the corresponding bulk materials. The Ms of 55 emu/g of magnetite nanoparticles in this study is better than the experimental value range of 30–50 emu/g (Gupta and Gupta, 2005). For synthesized magnetic nanoparticles, alginate can protect $Fe_3O_4$ of good magnetism from oxidizing to $Fe_2O_3$ of poor magnetism, since nanometer magnetite particles are very sensitive to the presence of oxygen and are rapidly oxidized to maghemite or to a magnetite–maghemite substitutional series. Moreover, based on AFM, $Fe_3O_4$ nanoparticles bound with alginate macromolecule strands, like "fruit" in the "tree", were visually confirmed. The good magnetism of the solid sample and suspension sample may contribute to the way $Fe_3O_4$ nanoparticles bind to alginate, not simply coated by polymer. If alginate coated the $Fe_3O_4$ nanoparticles completely, the magnetism would decrease significantly, since the effective hydrodynamic radius of the nanoparticles was much larger than their core radius (Denizot et al., 1999).

### 3.6. FT-IR analysis

The binding of $Fe_3O_4$ to alginate was also confirmed by FT-IR analysis. Fig. 7 shows FT-IR spectra of $Fe_3O_4$ particles, SPION-alginate and alginate (LVCR). FT-IR spectra of iron oxide exhibited strong bands in the low-frequency region (1000–500 $cm^{-1}$) due to the iron oxide skeleton. Depending on Fe(II) content, this pattern is consistent with the magnetite ($Fe_3O_4$) spectrum (band 570 $cm^{-1}$) or maghemite (γ-$Fe_2O_3$) spectrum (broad band 520–610 $cm^{-1}$), and in other regions, the spectra of iron oxide have weak bands (Nyquist and Kagel, 1971). It is obvious that the characteristic band of Fe-O at 572.95 $cm^{-1}$ appears in the FT-IR spectrum of $Fe_3O_4$ particles. As for the alginate (LVCR) spectrum, the carboxyl group of alginate has a single-band character of $\upsilon_{as}(COO^-)$ and $\upsilon_s(COO^-)$, and the values are 1716 $cm^{-1}$ and 1464 $cm^{-1}$, respectively. In the spectrum of SPION-alginate, $\upsilon_{as}(COO^-)$ and $\upsilon_s(COO^-)$

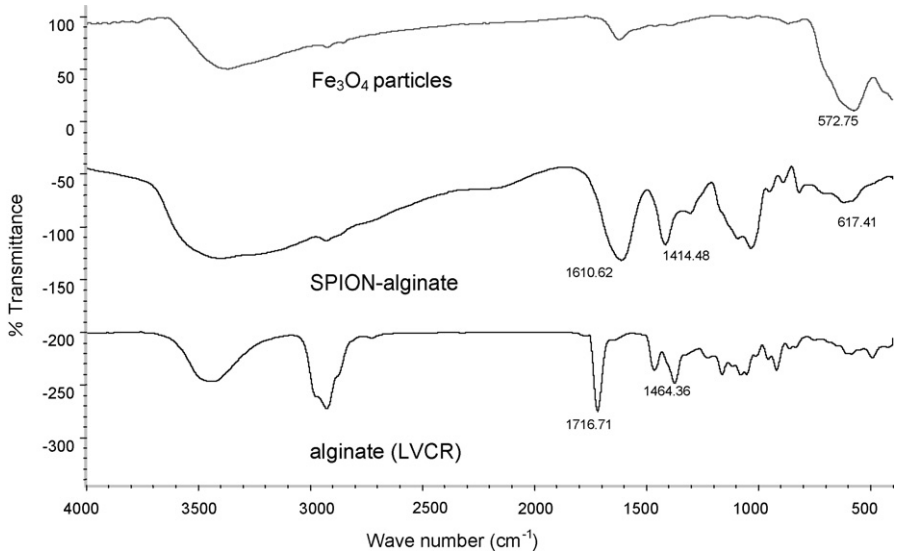


Fig. 7. FT-IR spectra of $Fe_3O_4$ particles, SPION-alginate and alginate (LVCR).

were shifted to lower frequencies of 1610 $cm^{-1}$ and 1414 $cm^{-1}$, and $\upsilon$(Fe-O) to a higher frequency of 617 $cm^{-1}$, suggesting that $Fe_3O_4$ was bound to alginate. This can be interpreted by assuming that the $COO^-$ terminal of alginate coordinates to Fe of $Fe_3O_4$ by complex formation. As a result, $Fe_3O_4$ nanoparticles were bound with alginate and this interaction might be as strong as a hydrogen bond, which also explains the high stability of SPION-alginate. If the interaction between $Fe_3O_4$ and alginate was only attributed to intermolecular force, $Fe_3O_4$ would dissociate from alginate and SPION-alginate would not be so stable.

### 3.7. T1 and T2 relaxivities

$T_1$-weighted and $T_2$-weighted images of SPION-alginate with different Fe concentrations are shown in Fig. 8. It is obvious that $T_1$-weighted images of SPION-alginate were brighter than that of the saline, while $T_2$-weighted images were darker. T1 relaxation times decreased from 1450 ms to 400 ms with increasing Fe concentration from 0.074 mM to 0.300 mM, while T2 relaxation times reduced from 40 ms to 10 ms. T1 and T2 relaxivities of SPION-alginate in saline (1.5 T, 20 °C) were $7.9 \pm 0.2\ s^{-1}\ mM^{-1}$ and $281.2 \pm 26.4\ s^{-1}\ mM^{-1}$ ($n = 3$), respectively, and the relative magnitude of T1 and T2 relaxivity was 35.7, indicating that SPION-alginate has moderate $T_1$ shortening and a strong $T_2$ shortening effect.

The enhancement of $R_1$ produced by iron oxides requires intimate contact between water molecules and the surface of iron oxide. The clustering of superparamagnetic crystals decreases the surface of iron oxide in contact with solvent; since T1 relaxivity is a function of the surface area, it decreases with

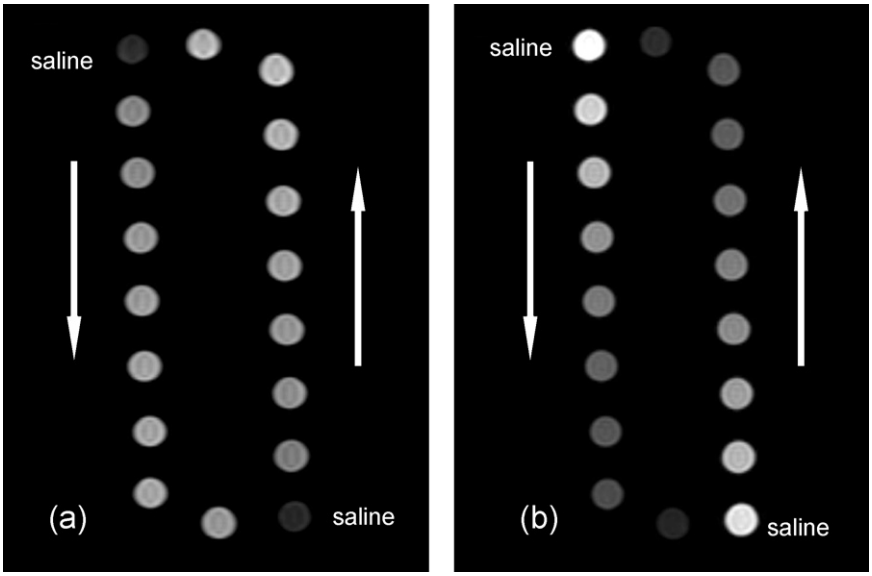


Fig. 8. $T_1$-weighted (a) and $T_2$-weighted (b) images of SPION-alginate in saline with Fe concentration from 0.0741 mM to 0.300 mM using an MRI scanner (1.5 T, 20 °C), and physiological saline was taken as a control sample.

increasing cluster size. The enhancement of T2 relaxivity reflects the ability of magnetic particles to distort the local magnetic field (Josephson et al., 1988).

Resovist® is a commercial MR contrast agent used clinically, of which the T1 and T2 relaxivities in blood (1.5 T, 37 °C) are $7.2 \pm 0.1\ s^{-1}\ mM^{-1}$ and $82.0 \pm 6.2\ s^{-1}\ mM^{-1}$, respectively. T1 relaxivity of SPION-alginate ($7.9 \pm 0.2\ s^{-1}\ mM^{-1}$) can be attributed to the fact that iron oxide was not coated by alginate, as confirmed by AFM, thus it makes iron oxide accessible in contact with water molecules. On the other hand, the higher T1 relaxivity of SPION-alginate ($281.2 \pm 26.4\ s^{-1}\ mM^{-1}$) indicates that it can produce strong local inhomogeneity in the applied magnetic field, hence allowing SPION-alginate at lower concentration to produce comparably in vivo effects on relaxation. Due to high T2 relaxivity, SPION-alginate is particularly suited to $T_2$-weighted imaging. Therefore, it can be used as a negative MR contrast agent.

## 4. Conclusions

SPION-alginate was prepared using a modified two-step coprecipitation method. The results revealed that typical iron oxide nanoparticles were $Fe_3O_4$ with a core diameter of 5–10 nm and SPION-alginate had a hydrodynamic diameter of 193.8–483.2 nm. Magnetic measurement showed that $Fe_3O_4$ nanoparticles in SPION-alginate were superparamagnetic with an Ms of 40 emu/g, corresponding to 73% of that of solid SPION-alginate (55 emu/g). This high Ms may be due to $Fe_3O_4$ nanoparticles binding with alginate macromolecule strands like "fruit" in the "tree", which was visually confirmed. SPION-alginate was very stable in size and $\xi$-potential at pH 7.0 for 12 months of storage at 4 °C. In addition, compared to other SPION preparations that have already been used clinically, SPION-alginate has a similar or lower T1 relaxivity while T2 relaxivity is very high. Hence, SPION-alginate may be used as a negative contrast agent.

## Acknowledgement

The authors are thankful to the National High Technology Research and Development Program of China (863 Program, No. 2003AA326020) for financial support of this study.

## References

Alexiou, C., Arnold, W., Klein, R.J., Parak, F.G., Hulin, P., Bergemann, C., Erhardt, W., Wagenpfeil, S., Lübbe, A.S., 2000. Locoregional cancer treatment with magnetic drug targeting. Cancer Res. 60, 6641–6648.

Bee, A., Massart, R., Neveu, S., 1995. Synthesis of very fine maghemite particles. J. Magn. Magn. Mater. 149, 6–9.

Bouhadir, K.H., Lee, K.Y., Alsberg, E., Damm, K.L., Anderson, K.W., Mooney, D.J., 2001. Degradation of partially oxidized alginate and its potential application for tissue engineering. Biotechnol. Prog. 17, 945–950.

Bulte, J.W., Douglas, T., Witwer, B., Zhang, S.C., Strable, E., Lewis, B.K., Zywicke, H., Miller, B., van Gelderen, P., Moskowitz, B.M., Duncan, I.D., Frank, J.A., 2001. Magnetodendrimers allow endosomal magnetic labeling and in vivo tracking of stem cells. Nat. Biotechnol. 19, 1141–1147.

Decho, A.W., 1999. Imaging an alginate polymer gel matrix using atomic force microscopy. Carbohydr. Res. 315, 330–333.

Denizot, B., Tanguy, G., Hindre, F., Rump, E., Jeune, J., Jallet, P., 1999. Phosphorylcholine coating of iron oxide nanoparticles. J. Colloid Interface Sci. 209, 66–71.

Drake, B., Prater, C.B., Weisenhorn, A.L., Gould, S.A., Albrecht, T.R., Quate, C.F., Cannell, D.S., Hansma, H.G., Hansma, P.K., 1989. Imaging crystals, polymers, and processes in water with atomic force microscope. Science 243, 1586–1589.

Finotelli, P.V., Morales, M.A., Rocha-Leão, M.H., Baggio-Saitovitch, E.M., Rossi, A.M., 2004. Magnetic studies of iron (III) nanoparticles in alginate polymer for drug delivery applications. Mater. Sci. Eng. C 24, 625–629.

Funovics, M.A., Kapeller, B., Hoeller, C., Su, H.S., Kunstfeld, R., Puig, S., Macfelda, K., 2004. MR imaging of the her2/neu and 9.2.27 tumor antigens using immunospecific contrast agents. Magn. Reson. Imaging 22, 843–850.

Gombotz, W.R., Wee, S.F., 1998. Protein release from alginate matrices. Adv. Drug Deliv. Rev. 31, 267–285.

Gupta, A.K., Gupta, M., 2005. Synthesis and surface engineering of iron oxide nanoparticles for biomedical applications. Biomaterials 26, 3995–4021.

Hagar, W., Vichinsky, E.P., Theil, E.C., 2003. Liver ferritin subunit ratios in neonatal hemochromatosis. Pediatr. Hematol. Oncol. 20, 229–235.

Jordan, A., Scholz, R., Maier-Hauff, K., Johannsen, M., Wust, P., Nadobny, J., Schirra, H., Schmidt, H., Deger, S., Loening, S., Lanksch, W., Felix, R., 2001. Presentation of a new magnetic field therapy system for the treatment of human solid tumors with magnetic fluid hyperthermia. J. Magn. Magn. Mater. 225, 118–126.

Josephson, L., Lewis, J., Jacobs, P., Hahn, P.F., Stark, D.D., 1988. The effects of iron oxides on proton relaxivity. Magn. Reson. Imaging 6, 647–653.

Kawaguchi, T., Hanaichi, T., Hasegawa, M., Maruno, S., 2001. Dextran-magnetite complex: conformation of dextran chains and stability of solution. J. Mater. Sci. 12, 121–127.

Khairou, K.S., Al-Gethami, W.M., Hassan, R.M., 2002. Kinetics and mechanism of sol–gel transformation between sodium alginate polyelectrolyte and some heavy divalent metal ions with formation of capillary structure polymembranes ionotropic gels. J. Membr. Sci. 209, 445–456.

Kroll, E., Winnik, F.M., Ziolo, R.F., 1996. In situ preparation of nanocrystalline $\gamma$-$Fe_2O_3$ in iron (II) cross-linked alginate gels. Chem. Mater. 8, 1594–1596.

Krotz, F., de Wit, C., Sohn, H.Y., Zahler, S., Gloe, T., Pohl, U., Plank, C., 2003. Magnetofection—a highly efficient tool for antisense oligonucleotide delivery in vitro and in vivo. Mol. Ther. 7, 700–710.

Llanes, F., Ryan, D.H., Marchessault, R.H., 2000. Magnetic nanostructured composites using alginates of different M/G ratios as polymeric matrix. Int. J. Biol. Macromol. 27, 35–40.

Massart, R., Dubois, E., Cabuil, V., Hasmonay, E., 1995. Preparation and properties of monodisperse magnetic fluids. J. Magn. Magn. Mater. 149, 1–5.

Medina, F., Segundo, C., Salcedo, I., Garcia-Poley, A., Brieva, J.A., 2004. Purification of human lamina propria plasma cells by an immunomagnetic selection method. J. Immunol. Methods 285, 129–135.

Nesterova, M.V., Walton, S.A., Webb, J., 2000. Nanoscale iron (III) oxyhydroxy aggregates formed in the presence of functional water-soluble polymers: models for iron(III) biomineralisation processes. J. Inorg. Biochem. 79, 109–118.

Neuberger, T., Schöpf, B., Hofmann, H., Hofmann, M., von Rechenberg, B., 2005. Superparamagnetic nanoparticles for biomedical applications: possibilities and limitations of a new drug delivery system. J. Magn. Magn. Mater. 293, 483–496.

Nishio, Y., Yamada, A., Ezaki, K., Miyashita, Y., Furukawa, H., Horie, K., 2004. Preparation and magnetometric characterization of iron oxide-containing alginate/poly(vinyl alcohol) networks. Polymer 45, 7129–7136.

Nyquist, R.A., Kagel, R.O., 1971. Infrared Spectra of Inorganic Compounds. Academic Press, New York, p. 219.

Olsvik, O., Popovic, T., Skjerve, E., Cudjoe, K.S., Hornes, E., Ugelstad, J., Uhlen, M., 1994. Magnetic separation techniques in diagnostic microbiology. Clin. Microbiol. Rev. 7, 43–54.

Ravi Kumar, M.N., Bakowsky, U., Lehr, C.M., 2004. Preparation and characterization of cationic PLGA nanospheres as DNA carriers. Biomaterials 25, 1771–1777.

Robitaille, R., Pariseau, J.F., Leblond, F.A., Lamoureux, M., Lepage, Y., Hallé, J.P., 1999. Studies on small (<350 μm) alginate-poly-L-lysine microcap-

sules. III. Biocompatibility of smaller versus standard microcapsules. J. Biomed. Mater. Res. 44, 116–120.

Shafi, K.V.P.M., Gedanken, A., Prozorov, R., Balogh, J., 1998. Sonochemical preparation and size-dependent properties of nanostructured $CoFe_2O_4$ particles. Chem. Mater. 10, 3445–3450.

Shen, F., Poncet-Legrand, C., Somers, S., Slade, A., Yip, C., Duft, A.M., Winnik, F.M., Chang, P.L., 2003. Properties of a novel magnetized alginate for magnetic resonance imaging. Biotechnol. Bioeng. 83, 282–292.

Simon, G.H., Bauer, J., Saborovski, O., Fu, Y., Corot, C., Wendland, M.F., Daldrup-Link, H.E., 2006. T1 and T2 relaxivity of intracellular and extracellular USPIO at 1.5 T and 3 T clinical MR scanning. Eur. Radiol. 16, 738–745.

Sipos, P., Berkesi, O., Tombácz, E., St Pierre, T.G., Webb, J., 2003. Formation of spherical iron (III) oxyhydroxide nanoparticles sterically stabilized by chitosan in aqueous solutions. J. Inorg. Biochem. 95, 55–63.

Sonvico, F., Mornet, S., Vasseur, S., Dubernet, C., Jaillard, D., Degrouard, J., Hoebeke, J., Duguet, E., Colombo, P., Couvreur, P., 2005. Folate-conjugated iron oxide nanoparticles for solid tumor targeting as potential specific magnetic hyperthermia mediators: synthesis, physicochemical characterization, and in vitro experiments. Bioconjugate Chem. 16, 1181–1188.

Sreeram, K.J., Yamini Shrivastava, H., Nair, B.U., 2004. Studies on the nature of interaction of iron (III) with alginates. BBA-Gen Subj. 1670, 121–125.

Suwa, T., Ozawa, S., Ueda, M., Ando, N., Kitajima, M., 1998. Magnetic resonance imaging of esophageal squamous cell carcinoma using magnetite particles coated with anti-epidermal growth factor receptor antibody. Int. J. Cancer 75, 626–634.

Upadhyay, R.V., Davies, K.J., Wells, S., Charles, S.W., 1995. Preparation and characterization of ultra-fine $MnFe_2O_4$ and $Mn_xFe_{1-x}O_4$ spinel systems: II. Magnetic fluids. J. Magn. Magn. Mater. 139, 249–254.

Vijayakumar, R., Koltypin, Y., Felner, I., Gedanken, A., 2000. Sonochemical synthesis and characterization of pure nanometer-sized $Fe_3O_4$ particles. Mater. Sci. Eng. A 286, 101–105.

Wan, M.X., Zhou, W.X., Li, J.C., 1996. Composite of polyaniline containing iron oxides with nanometer size. Synth. Met. 78, 27–31.

Wang, Y.X., Hussain, S.M., Krestin, G.P., 2001. Superparamagnetic iron oxide contrast agents: physicochemical characteristics and applications in MR imaging. Eur. Radiol. 11, 2319–2331.